HHS Public Access

Author manuscript

Sens Actuators B Chem. Author manuscript; available in PMC 2020 May 01.

Published in final edited form as:

Sens Actuators B Chem. 2020 May 1; 310: . doi:10.1016/j.snb.2020.127838.

A Robust Bioderived Wavelength-Specific Photosensor Based on BLUF Proteins

Jing Tong[a,b], **Peng Zhang**[e], **Lei Zhang**[c,d], **Dongwei Zhang**[c,d], **David N. Beratan**[e,f,g], **Haifeng Song**[c,d,*], **Yi Wang**[c,d,*], **Tie Li**[a,*]

[a]Science and Technology on Microsytem Laboratory, Shanghai Institute of Microsystem and Information Technology, Chinese Academy of Sciences, Shanghai 200050, China

[b]University of Chinese Academy of Sciences (UCAS), Beijing 100049, China

[c]State Key Laboratory of Proteomics, National Center for Protein Sciences (Beijing), Beijing Institute of Lifeomics, Beijing 102206, China

[d]National engineering research center for protein drugs (NERCPD), Beijing 102206, China

[e]Department of Chemistry, Duke University, Durham, North Carolina 27708, United States

[f]Department of Physics, Duke University, Durham, North Carolina 27708, United States

[g]Department of Biochemistry, Duke University Medical Center, Durham, North Carolina 27710, United States

Abstract

Photosensitive proteins are naturally evolved photosensors that often respond to light signals of specific wavelengths. However, their poor stability under ambient conditions hinders their applications in non-biological settings. In this proof-of-principle study, we grafted the blue light using flavin (BLUF) protein reconstructed with flavin adenine dinucleotide (FAD) or roseoflavin (RoF) onto pristine graphene, and achieved selective sensitivity at 450 nm or 500 nm, respectively. We improved the thermal and operational stability substantially via structure-guided cross-linking, achieving 6-month stability under ambient condition and normal operation at temperatures up to 200 °C. Furthermore, the device exhibited rare negative photoconductivity behavior. The origins of this negative photoconductivity behavior were elucidated via a combination of experimental and theoretical analysis. In the photoelectric conversion studies, holes from photoexcited flavin migrated to graphene and recombined with electrons. The device allows facile modulation and detection of charge transfer, and provides a versatile platform for future studies of photoinduced charge transfer in biosensors as well as the development of stable wavelength-selective biophotosensors.

Graphical Abstract

*Corresponding author: songhf@vip.163.com, wangy@serene-t.com, tli@mail.sim.ac.cn.

Supporting Information

The supporting information containing details of the MD simulations, Table S1–S3 and Figure S1–S6 is available free of charge on the website.

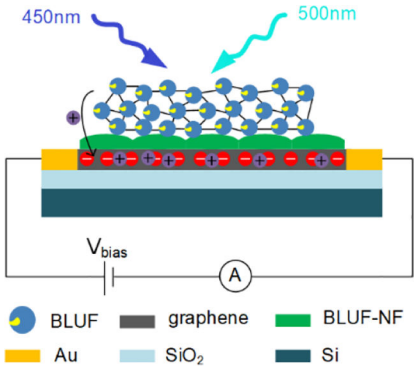

A graphene-based thermally stable and operationally stable biosensor for detecting specific wavelengths is proposed.

Keywords

biosensor; graphene; photodetection; photosensitive proteins; blue light using flavin; charge transfer

1. Introduction

Photosensitive proteins possess a wide variety of light-induced biochemical or biophysical characteristics, such as strong and highly specific optical response [1–4]. We witnessed a history of biomolecule-based photoelectronic device from the 1980s when bacteriorhodopsin was used to produce photoswitchable capacitors and memories [5, 6] to recent booming field of photodetectors containing complex photosynthesis systems [7, 8]. However, they are susceptible to a variety of deactivation pathways in both aqueous and solid-state structures [9] (Bacteriorhodopsin is a robust exception). Many techniques exist to address stability issues in protein-based biosensors, including non-specific covalent cross-linking, physical entrapment and hydrogel protection [10–15]. Nonetheless, approaches to realize improving stabilities of solid-state biophotosensors are not widely available [16, 17].

Here, we hypothesize that wavelength-selective photoconductive devices may be constructed with substantially improved stability by: 1) reconstituting photosensitive proteins with wavelength-selective chromophores; 2) using structure-directed mutagenesis to facilitate extensive cross-linking and formation of multilayered structure; 3) protecting the sensor surface with a transparent polymeric film; and 4) adding a biocompatible mediator layer between the sensing protein and the underlying nanomaterial. Highly cross-linked and multilayer structures may retain sufficient transparency, while benefiting from high density of sensitive units for enhanced stability and sensitivity. Complete isolation of the sensing protein from the environment above the film may further improve its stability without sacrificing its accessibility to light. The selection of photosensitive protein is based upon three criteria: 1) the protein's intrinsic biological function involves a physical response to light of specific wavelength, with light-induced conformational change and/or light-induced charge transfer; 2) the protein has a simple and well understood structure that is amenable to

prokaryotic overexpression and site-directed mutagenesis; 3) the protein is stable in solution and in dried form.

We tested our hypotheses on a photosensor platform with pristine graphene, and selected the blue light using flavin (BLUF) protein from photosensor protein AppA [18–22] as the photosensitive protein. Compared to other photosensitive proteins (cryptochrome, bacteriophytochrome, etc.), BLUF is a small protein (14 kDa) with a simple “sandwich-like” structure [18–22]. Excitation of BLUF by 450 nm light gives rise to proton-coupled electron transfer (PCET) from the conserved Tyr21 to flavin, inducing local rearrangement of hydrogen bonds and global conformational change in the protein [20]. The resulting biosensor was highly sensitive to 450 nm light (FAD) or 500 nm light (roseoflavin, RoF [23, 24]). It also exhibited unusually high thermal stability (up to 200 °C) and showed outstanding stability for 6-month at ambient conditions. Intriguingly, the light sensing in our device is mediated by a rare negative photoconductivity (NPC) mechanism in which incident photons diminish the current [25, 26]. With site-directed mutagenesis and computational simulations, we delineate a novel NPC mechanism in which photoexcited BLUF proteins inject holes into graphene that then recombine with free electrons. As a consequence of this, the photoconductivity of the device decreases upon illumination. Surprisingly, the intrinsic charge transfer pathway of BLUF did not contribute to the observed signal transduction mechanism, but served as a diverging route that limits the signal strength. Our BLUF-graphene hybrid sensor is not only a proof-of-concept system for our design principles, but may also be used as a simple system to study light driven charge transfer through proteins.

2. Experimental

2.1 Materials and chemicals

The single layer graphene films were prepared by chemical vapor deposition (2D Carbon, China) on copper films. The phosphate-buffered saline (PBS), N-(3-dimethylaminopropyl)-N-ethylcarbodiimide hydrochloride crystalline (EDC), N-hydroxysuccinimide (NHS), 4-morpholineethanesulfonic acid (MES) and roseoflavin (RoF) were purchased from Sigma-Aldrich (USA). Ethanolamine, flavin adenine dinucleotide (FAD) and flavin mononucleotide (FMN) were purchased from TCI Chemicals (Japan). Polydimethylsiloxane (PDMS) was purchased from Dow (USA). All solutions used in this study were filtered by 0.22 μm filters (Merck Millipore, Germany) prior to use.

2.2 Protein expression and purification

The wildtype and mutant BLUF genes were cloned into the expression vector pET28a via restriction sites BamHI/XhoI. Mutants (listed in Table S1) were prepared by site-directed mutagenesis. E. coli strain BL21-DE3 carrying either the wildtype or mutant BLUF genes was cultured in LB media and the expression was induced by 0.7 mM IPTG for 18 h at 18 °C. Cells were harvested and lysed with sonication in binding buffer (50 mM Tris-HCl, pH 8.0, 200 mM NaCl). After centrifugation, the his-tagged BLUF protein was first purified by Ni-NTA affinity chromatography. The protein was then subjected to complete denaturing in 6 M guanidine hydrochloride, which was then refolded via dialysis against a step gradient of 3 M and 1.5 M guanidine hydrochloride at 4 °C for 12 h, in the presence of either FAD,

FMN or roseoflavin. Finally, the protein solution was dialyzed into PBS. The reconstructed monomeric BLUF protein was further purified by anion exchange with QFF column (GE LifeSciences, USA) and size exclusion chromatography with HiLoad 16/60 Superdex 75 column (GE LifeSciences, USA). The purified protein was stored at −80 °C for further use.

2.3 Fabrication of the graphene photodetector substrate and surface modification

The fabrication process is shown in Figure 1. Firstly, a 300 nm thick SiO_2 layer was grown on Si substrate through dry oxygen oxidation. Interdigital electrodes (Ti/Au, 20 nm/200 nm) were then deposited onto the SiO_2/Si substrate by lift off process. The graphene film was transferred onto the interdigital electrodes through a PMMA (poly(methyl methacrylate))-based method. The surface of graphene was then cleaned by thermal annealing in Ar/H_2 atmosphere at 300 °C for one hour. The graphene photodetector substrate was incubated in BLUF-NF (BLUF devoid of the flavinyl cofactor) solution (20 μM) for 3 min at 80 °C to introduce carboxylic acid groups onto the surface (Figure 1a), followed by a deionized water rinse. The carboxylic acid groups were then activated with a solution of 0.4 M EDC and 0.1 M NHS in 0.1 M MES buffer pH 5.2 for 1 h at room temperature. After that, the device was rinsed in 0.1 M MES (pH 5.2). In order to covalently immobilize BLUF on the graphene surface, the device was exposed to a 1:1 mixture of 20 μM BLUF in PBS solution, and 0.4 M EDC with 0.1 M NHS in 0.1 M MES buffer (pH 5.2) overnight at 4 °C. After immobilization, the surface was rinsed with 1×PBS solution (pH 7.4). To further quench the reaction and block excess reactive groups, the surface was immersed in the PBS solution of ethanolamine (1 mM, pH 7.4) for 20 min. Finally, the BLUF modified device was rinsed with deionized water, dried and stored under N_2 for further use (Figure 1b). To protect the sensing protein layer, PDMS was spin-coated onto the surface and completely cured at room temperature for 24 h.

2.4 Sensing apparatus and parameters

All electrical measurements were conducted using a Keithley 4200 semiconductor parameter analyzer (Keithley Instruments Inc., Cleveland, OH). The light sensing measurements were conducted using a UV-Vis LED light source (BJ Jing Zhen Da Tec., China) with wavelength of 450 nm, 500 nm, 600 nm, 640 nm, 675 nm, 742 nm and 800 nm respectively. Atomic force microscopy (Dimension Icon, Bruker, USA) was used to determine the thickness and surface topology of the graphene films before and after functionalization. Raman spectra (DXR, Thermo Fisher, USA) were obtained to explore the interactions between graphene and protein. X-ray photoelectron spectroscopy (Escalab250Xi, Thermo Fisher, USA) was used to verify the elemental composition of the modified graphene surface.

3. Results and discussion

3.1 Sensor characterization

Thermal annealing was performed using hydrogen gas and argon gas to remove residual reagents and reduce the graphene film. The vminimum thickness of the graphene film transferred on the electrode (0.4 nm) was measured using AFM (Figure 2a), which is consistent with the typical thickness of the observed single layer graphene sheet (0.335 nm) [27]. The large surface roughness was due to the nucleation on the polycrystalline graphene,

resulting in an average thickness (1 nm) higher than the theoretical value of the single layer graphene. Raman spectroscopy is an effective non-destructive method for determining the number of layers and the structural integrity of graphene sheets. The low D/G ratio of pristine graphene (Figure 2d) showed that the graphene film had few defects and clean surface.

In order to mitigate the nanotoxicity [28] arising from direct contact between BLUF and the hydrophobic graphene surface, we introduced a heat-denatured film of BLUF-NF between graphene and the light sensing BLUF layer, similar to the approach developed by Zhou et al. [29] In the XPS spectra, the single C1s peak of pristine graphene (Figure 2e) morphed into a compound peak of multiple origins (Figure 2f), indicative of successful BLUF-NF protein modification. The binding energy of 284.8 eV is attributed to sp^2-hybridized C in C-C bonds. The binding energy of 286.1 eV corresponded to the carbon atoms in C-S bonds, which is an effective feature of the modification of BLUF-NF. And the binding energy at approximately 288.1 eV arose from the carbonyl carbon atoms on the denatured BLUF-NF film, indicating −COOH bonds and −CO-NH bonds. The contact angle decreased from 93.1° to 54.6° after the BLUF-NF functionalization (Figure S1). It suggested that the exposed hydrophobic residues of the thermal denatured BLUF-NF contacted the hydrophobic graphene surface, while the highly hydrophilic areas faced upward. The increased hydrophilicity prevented further stacking of denatured BLUF-NF, leaving a monolayer of 3.5 nm thickness (Figure 2b) and a biocompatible surface. Over 10% of BLUF's amino acid residues are either Asp or Glu, which orient away from the graphene surface. Thus, the BLUF-NF film not only served as an intermediate layer to improve the BLUF stability, but also functionalized the graphene with a large number of carboxylate groups.

To graft the native BLUF onto the BLUF-NF monolayer, we chose a multilayer immobilization scheme instead of a self-assembled monolayer (SAM) strategy. Since light sensing does not require direct contact between the sensing layer and the "analyte" (i.e., the incident light), maximizing the density of light-sensitive units on the graphene surface is the primary goal. Before drop-casting, we premixed NHS and EDC•HCl with BLUF to promote extensive cross-linking, while allowing the BLUF amine groups to react with surface bound NHS-esters. Although wildtype BLUF contains 14 carboxylic groups, there is only one lysyl amine. We therefore mutated four of the 19 Arg residues into Lys, guided by the crystal structure (PDB ID: 2IYI [30], R47K, R81K, R98K and R116K), which we refer to as BLUF-K_5. Positioning five Lys residues on the surface of BLUF-K_5 allowed NHS-EDC coupling to occur in multiple directions. Overnight incubation of BLUF-K_5 with the BLUF-NF-NHS-ester surface created a 12 nm film (Figure 2c) of cross-linked BLUF-K_5 roughly producing a double-layer.

3.2 Sensing performance

Figure 3a shows the results induced by exposure to 450 nm light for 100 s for differentially functionalized devices (the light power used in this study was 35 mW•cm^{-2} unless otherwise noted). For the pristine graphene device, the 450 nm light induced little change of the device current, most likely due to graphene's low absorptivity of light. The current of the device modified with cross-linked BLUF-K_5 decreased by 14% upon illumination of 450 nm light,

three times more strongly than that of the device modified with BLUF-K_5 SAM. Unsurprisingly, the device with native BLUF-NF showed little response to 450 nm light, due to the absence of the flavin cofactor. When the free FAD was drop-cast at equimolar concentration to BLUF-K_5, which presumably left equal (if not more) blue-light-sensitive moieties on the surface, the photoresponse was negligible (Figure S2). The structure of FAD embedded in the BLUF protein is essential for the device' photoresponse. We then exposed the BLUF-K_5 device to 450 nm light of six different intensities, 0.33 mW•cm^{-2}, 5 mW•cm^{-2}, 10 mW•cm^{-2}, 21.7 mW•cm^{-2}, 35 mW•cm^{-2} and 48.6 mW•cm^{-2} respectively. There is a linear relationship between the light intensity and photocurrent amperage, with an average photoresponse of −19.64 mA•W^{-1} (Figure 3b). Further, the device can detect light as weak as 0.33 mW•cm^{-2}.

We next investigated the device's wavelength selectivity. In contrast to the rather broad absorption spectrum of free FAD between 450 nm and 500 nm (Figure S3), BLUF-K_5 had a strong absorption of 450 nm light in solution (Figure 4a). The absorption maximum of RoBLUF obtained by reconstituting BLUF through roseoflavin (Figure S4) was shifted to 500nm. Graphene photosensors were illuminated with equienergetic lights of seven wavelengths, ranging from 450 nm to 800 nm. The device with only pristine graphene did not exhibit response to any wavelength within this range. Consistent with BLUF-K_5's solution phase absorption spectrum, the highest wavelength sensitivity BLUF-K_5 device is located at 450 nm. For the RoBLUF device, we observed a weaker (compared to the BLUF-K_5 device) but highly specific response to the 500 nm light. Even the 450 nm light, in which the photon carries more energy than that of the 500 nm light, did not illicit any response in the RoBLUF device, demonstrating that the solution phase biospecificity is well retained in the solid phase.

The multilayer and cross-linked structure of the device also conferred the BLUF-K_5 device with significantly enhanced stability. We fabricated the device using a micro-heat chip [31] to investigate the device's performance at elevated temperatures. The device retained sensitivity and wavelength selectivity at temperatures as high as 200 °C (Figure 5a), while the protein lost structural integrity above 55 °C in aqueous solution (Figure S5). As shown in Figure 5b, the graphene photosensors functionalized with free FAD or with cross-linked BLUF-NF still maintained a low photoresponse at high temperatures. We attributed this unusually high thermal stability to the extensive network of intermolecular amide bonds which tightly locked the BLUF monomers in their native conformation. This resistance to heating may be of use in the future for parallel biomolecular functionalization on a wafer, which would substantially improve the reproducibility of biosensor chips. To address the issue of rapid device degradation with time, we further protected the light sensitive biolayer using a transparent PDMS film. The polymerization reaction did not impair light sensing activity of BLUF. When stored at ambient conditions, the protected device exhibited consistent performance (signal intensity and wavelength selectivity) for six months (Figure 5c).

3.3 Sensing mechanism

To investigate the mechanism of operation for the device, we first determined the mode of signal transduction in BLUF. There are two probable mechanisms for photoexcited BLUF to cause a decrease in electric current: electrostatic gating or charge transfer. Electrostatic gating may arise from protein conformational changes between the dark and light states of BLUF, induced by rearrangement of hydrogen bonding network around flavin [20, 22, 32–34]. The electrostatic perturbation from a protein conformational change may gate the conductivity of graphene. Charge transfer between the photoexcited FAD and graphene may also affect the device current. To examine these competing mechanisms, we functionalized the graphene with the BLUF-K_5-W104A mutant, which was previously shown to recover more rapidly than BLUF-K_5 following photoexcitation in solution [34]. Electrostatic gating effects should manifest as faster recovery in the BLUF-K_5-W104A device than in the BLUF-K_5 device. The recovery rates of the two devices were identical (Figure S6), suggesting that the charge transfer mechanism may account for the light-induced response.

To identify the photogenerated charge carriers, we constructed a liquid-gated GFET device functionalized with BLUF-K_5 (Figure 6a). The Dirac point of pristine graphene was shifted from 0 V to −0.3 V after BLUF functionalization (Figure 6b), consistent with n-doping. GFET is a bipolar field field effect transistor. The graphene as a channel exhibits a p or n type property as the gate voltage changes. We measured the output characteristics of the GFET device under illumination at different gate voltages. When the majority carriers were holes (gate-source bias, V_{gs} was −0.8 V), the drain-source current (I_{ds}) increased with 450 nm illumination, indicative of holes migrating from FAD to graphene (Figure 6c). When the majority carriers were electrons (V_{gs} = −0.1 V), light illumination led to a decrease of I_{ds}, again suggesting injection of holes into graphene. Illumination with 640 nm light of equal power failed to elicit any change in the source-drain current. Previous biophysical studies of BLUF indicated that the intrinsic PCET process involved holes migrating from flavin to proximal amino acid residues [18, 19, 35–37]. Thus, the observed negative photoconductivity likely arose from photoexcited BLUF injecting holes into the n-doped graphene, decreasing the majority charge carrier density.

We studied sensor performance with a series of BLUF mutants to elucidate the hole-transfer pathways. Surface lysine residues were the most likely hole mediators from FAD to graphene through the protein. We mutated each of the five surface Lys residues to Arg in order to break one of the five potential covalent BLUF-BLUF and BLUF-graphene connections. Figure 6d shows that the removal of Lys98 and 116 did not affect the magnitude of the current drop upon illumination, while mutations of Lys32, 47 and 81 decreased the signal. Electron tunneling pathway [38–40] analysis from FAD to the five BLUF-K_5 Lys residues showed that the photogenerated holes at FAD couple strongly to the three proximal lysine residues (Lys32, 47 and 81), mediated by one to three intervening residues, while couplings to Lys98 and to Lys116 were weaker (by two orders of magnitude) as compared to other Lys due to the longer tunneling distances (Table S2). The weaker couplings to Lys98 and 116 explain the invariant light-induced current drops upon removing these residues. The details of the tunneling pathway analysis are reported in the supporting information.

In the intrinsic charge transfer pathway of BLUF, Tyr21 is the key proton and electron donor of the PCET reaction. We prepared the BLUF-K_5-Y21I mutant protein for device fabrication with the anticipation of a complete loss of sensitivity to 450 nm light. To our surprise, the device exhibited a stronger response to 450 nm light than did the BLUF-K_5 device (Figure 6d). The productive pathways from FAD to Lys32, 47 or 81 did not involve Tyr21 (Table S3). Rather, Tyr21 is positioned so that the intrinsic charge transfer from FAD to Tyr21 and Trp104 may divert the flux of holes and contribute negatively to the signal transduction. Thus, the Y21I mutation most likely shuts off one of the major diverging pathways, redirecting more holes to the underlying graphene.

4. Conclusions

In summary, we developed a highly stable biophotosensor by multi-step functionalization of graphene with heat denatured BLUF-NF and cross-linked BLUF-K_5, achieving a strong and selective response to 450/500 nm light. Heat-denatured BLUF-NF as an interfacial mediator improved the biocompatibility of graphene and facilitated protein immobilization. The device operated normally at 200 °C and lasted for six months when protected by PDMS. Site-directed mutagenesis and electron tunneling pathway analysis identified a probable set of coupling pathways for holes hopping from the photoexcited flavin to the graphene, giving rise to the observed NPC. This mechanism may arise in other light-sensitive proteins that are potential candidates for development as wavelength-selective biosensors. This device platform is also a highly tunable, robust and low-cost system for the study of photo-induced protein-mediated charge transfer.

Supplementary Material

Refer to Web version on PubMed Central for supplementary material.

Acknowledgements

We appreciate financial support from the Project of National Natural Science Foundation of China (No. 31400733, 91323304, 61327811), the National Key Research and Development Program of China (No. 2018YFA0208500, No. 2017YFA0207103 and 2017YFB0405403), Project for Shanghai Outstanding Academic Leaders (15XD1504300). DNB and PZ acknowledge NIH grant GM-48043 for support.

References

[1]. Moglich A, Yang XJ, Ayers RA, Moffat K, Structure and Function of Plant Photoreceptors, in: Merchant S, Briggs WR, Ort D (Eds.), Annual Review of Plant Biology, Vol 61, Annual Reviews, Palo Alto, 2010, pp. 21–47.

[2]. Nakamaru S, Scholz F, Ford WE, Goto Y, von Wrochem F, Photoswitchable Sn-Cyt c Solid-State Devices, Adv Mater, 29(2017) 5.

[3]. Nelson N, Junge W, Structure and Energy Transfer in Photosystems of Oxygenic Photosynthesis, in: Kornberg RD (Ed.) Annual Review of Biochemistry, Vol 84, Annual Reviews, Palo Alto, 2015, pp. 659–83.

[4]. Rodriguez EA, Campbell RE, Lin JY, Lin MZ, Miyawaki A, Palmer AE, et al., The Growing and Glowing Toolbox of Fluorescent and Photoactive Proteins, Trends Biochem Sci, 42(2017) 111–29. [PubMed: 27814948]

[5]. Hampp N, Bacteriorhodopsin as a photochromic retinal protein for optical memories, Chem Rev, 100(2000) 1755–76. [PubMed: 11777419]

[6]. Jin YD, Honig T, Ron I, Friedman N, Sheves M, Cahen D, Bacteriorhodopsin as an electronic conduction medium for biomolecular electronics, Chem Soc Rev, 37(2008) 2422–32. [PubMed: 18949115]

[7]. Gong Y, Liu Q, Gong M, Wang T, Zeng G, Chan W-L, et al., High-Performance Photodetectors Based on Effective Exciton Dissociation in Protein-Adsorbed Multiwalled Carbon Nanotube Nanohybrids, Advanced Optical Materials, 5(2017).

[8]. Das R, Kiley PJ, Segal M, Norville J, Yu AA, Wang LY, et al., Integration of photosynthetic protein molecular complexes in solid-state electronic devices, Nano Lett, 4(2004) 1079–83.

[9]. Kim Y, Shin SA, Lee J, Yang KD, Nam KT, Hybrid system of semiconductor and photosynthetic protein, Nanotechnology, 25(2014) 20.

[10]. Bhakta SA, Evans E, Benavidez TE, Garcia CD, Protein adsorption onto nanomaterials for the development of biosensors and analytical devices: A review, Anal Chim Acta, 872(2015) 7–25. [PubMed: 25892065]

[11]. Erokhin V, Facci P, Nicolini C, 2-DIMENSIONAL ORDER AND PROTEIN THERMAL-STABILITY - HIGH-TEMPERATURE PRESERVATION OF STRUCTURE AND FUNCTION, Biosens Bioelectron, 10(1995) 25–34.

[12]. Gibson TD, Woodward JR, PROTEIN STABILIZATION IN BIOSENSOR SYSTEMS, Acs Symposium Series, 487(1992) 40–55.

[13]. Liebana S, Drago GA, Bioconjugation and stabilisation of biomolecules in biosensors, in: Estrela P (Ed.) Biosensor Technologies for Detection of Biomolecules, Portland Press Ltd, London, 2016, pp. 59–68.

[14]. Scouten WH, Luong JHT, Brown RS, Enzyme or protein immobilization techniques for applications in biosensor design, Trends Biotechnol, 13(1995) 178–85.

[15]. Tello A, Cao R, Marchant MJ, Gomez H, Conformational Changes of Enzymes and Aptamers Immobilized on Electrodes, Bioconjugate Chem, 27(2016) 2581–91.

[16]. Stieger KR, Ciornii D, Kolsch A, Hejazi M, Lokstein H, Feifel SC, et al., Engineering of supramolecular photoactive protein architectures: the defined co-assembly of photosystem I and cytochrome c using a nanoscaled DNA-matrix, Nanoscale, 8(2016) 10695–705. [PubMed: 27150202]

[17]. Yang SY, Robinson MT, Mwambutsa F, Cliffel DE, Jennings GK, Effect of Cross-linking on the Performance and Stability of Photocatalytic Photosystem I Films, Electrochim Acta, 222(2016) 926–32.

[18]. Fudim R, Mehlhorn J, Berthold T, Weber S, Schleicher E, Kennis JTM, et al., Photoinduced formation of flavin radicals in BLUF domains lacking the central glutamine, FEBS J, 282(2015) 3161–74. [PubMed: 25880920]

[19]. Jung A, Domratcheva T, Tarutina M, Wu Q, Ko WH, Shoeman RL, et al., Structure of a bacterial BLUF photoreceptor: Insights into blue light-mediated signal transduction, Proc Natl Acad Sci USA, 102(2005) 12350–5. [PubMed: 16107542]

[20]. Masuda S, Light Detection and Signal Transduction in the BLUF Photoreceptors, Plant Cell Physiol, 54(2013) 171–9. [PubMed: 23243105]

[21]. Masuda S, Hasegawa K, Ono T, Light-induced structural changes of apoprotein and chromophore in the sensor of blue light using FAD (BLUF) domain of AppA for a signaling state, Biochemistry, 44(2005) 1215–24. [PubMed: 15667215]

[22]. Mathes T, van Stokkum IHM, Stierl M, Kennis JTM, Redox Modulation of Flavin and Tyrosine Determines Photoinduced Proton-coupled Electron Transfer and Photoactivation of BLUF Photoreceptors, J Biol Chem, 287(2012) 31725–38. [PubMed: 22833672]

[23]. Mathes T, Vogl C, Stolz J, Hegemann P, In Vivo Generation of Flavoproteins with Modified Cofactors, J Mol Biol, 385(2009) 1511–8. [PubMed: 19027027]

[24]. Zirak P, Penzkofer A, Mathes T, Hegemann P, Absorption and emission spectroscopic characterization of BLUF protein Slr1694 from Synechocystis sp PCC6803 with roseoflavin cofactor, Journal of Photochemistry and Photobiology B-Biology, 97(2009) 61–70.

[25]. Baek E, Rim T, Schutt J, Baek CK, Kim K, Baraban L, et al., Negative Photoconductance in Heavily Doped Si Nanowire Field-Effect Transistors, Nano Lett, 17(2017) 6727–34. [PubMed: 28961014]

[26]. Yang YM, Peng XY, Kim HS, Kim T, Jeon S, Kang HK, et al., Hot Carrier Trapping Induced Negative Photoconductance in InAs Nanowires toward Novel Nonvolatile Memory, Nano Lett, 15(2015) 5875–82. [PubMed: 26226506]

[27]. Akhavan O, The effect of heat treatment on formation of graphene thin films from graphene oxide nanosheets, Carbon, 48(2010) 509–19.

[28]. Zuo GH, Kang SG, Xiu P, Zhao YL, Zhou RH, Interactions Between Proteins and Carbon-Based Nanoparticles: Exploring the Origin of Nanotoxicity at the Molecular Level, Small, 9(2013) 1546–56. [PubMed: 23038664]

[29]. Zhou L, Wang K, Wu ZH, Dong HD, Sun H, Cheng XH, et al., Investigation of Controllable Nanoscale Heat-Denatured Bovine Serum Albumin Films on Graphene, Langmuir, 32(2016) 12623–31. [PubMed: 27934532]

[30]. Jung A, Reinstein J, Domratcheva T, Shoeman RL, Schlichting I, Crystal structures of the AppA BLUF domain photoreceptor provide insights into blue light-mediated signal transduction, J Mol Biol, 362(2006) 717–32. [PubMed: 16949615]

[31]. Guo LF, Li T, Sub-ppb and ultra selective nitrogen dioxide sensor based on sulfur doped graphene, Sensors and Actuators B-Chemical, 255(2018) 2258–63.

[32]. Conrad KS, Manahan CC, Crane BR, Photochemistry of flavoprotein light sensors, Nat Chem Biol, 10(2014) 801–9. [PubMed: 25229449]

[33]. Losi A, Flavin-based blue-light photosensors: A photobiophysics update, Photochem Photobiol, 83(2007) 1283–300. [PubMed: 18028200]

[34]. Masuda S, Hasegawa K, Ono TA, Tryptophan at position 104 is involved in transforming light signal into changes of beta-sheet structure for the signaling state in the BLUF domain of AppA, Plant Cell Physiol, 46(2005) 1894–901. [PubMed: 16204305]

[35]. Gauden M, van Stokkum IHM, Key JM, Luhrs DC, Van Grondelle R, Hegemann P, et al., Hydrogen-bond switching through a radical pair mechanism in a flavin-binding photoreceptor, Proc Natl Acad Sci USA, 103(2006) 10895–900. [PubMed: 16829579]

[36]. Hammes-Schiffer S, Stuchebrukhov AA, Theory of Coupled Electron and Proton Transfer Reactions, Chem Rev, 110(2010) 6939–60. [PubMed: 21049940]

[37]. Migliore A, Polizzi NF, Therien MJ, Beratan DN, Biochemistry and Theory of Proton-Coupled Electron Transfer, Chem Rev, 114(2014) 3381–465. [PubMed: 24684625]

[38]. Antony J, Medvedev DM, Stuchebrukhov AA, Theoretical study of electron transfer between the photolyase catalytic cofactor FADH(−) and DNA thymine dimer, J Am Chem Soc, 122(2000) 1057–65.

[39]. Beratan DN, Onuchic JN, Electron tunneling pathways in proteins: influences on the transfer rate, Photosynth Res, 22(1989) 173. [PubMed: 24424807]

[40]. Betts JN, Beratan DN, Onuchic JN, Mapping Electron Pathways: An algorythm that finds the “minimum length”/maximum coupling pathway between electron donors and acceptors in proteins, J Am Chem Soc, 114(1992) 4043–6.

Highlights

- By incorporating photosensitive proteins reconstituted with different chromophores, we fabricated biophotosensors with distinct wavelength selectivities.
- The stability of this biophotosensor was significantly improved through a series of novel functional methods.
- Oriented movement of photogenerated holes from FAD to graphene caused the device to exhibit negative photoconductivity.

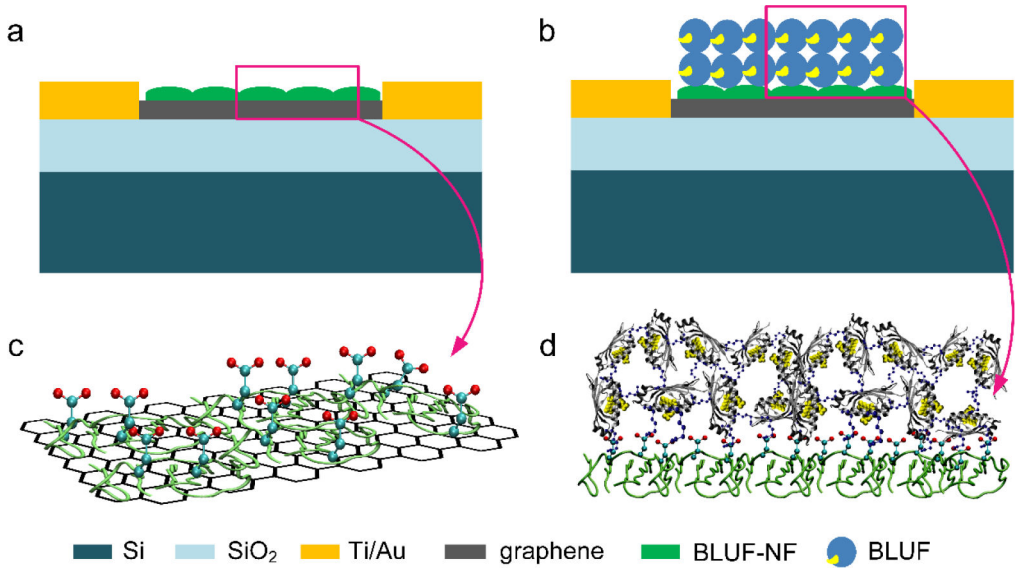

Figure 1.

Schematic depicting various steps involved in the fabrication of BLUF based graphene photosensor. (a) Thermally denatured BLUF-NF thin film adsorbed onto and functionalized the graphene sheet with carboxylic groups. (b) A double-layer of cross-linked penta-lysine-mutant of BLUF (BLUF-K_5) attached to the BLUF-NF thin film.

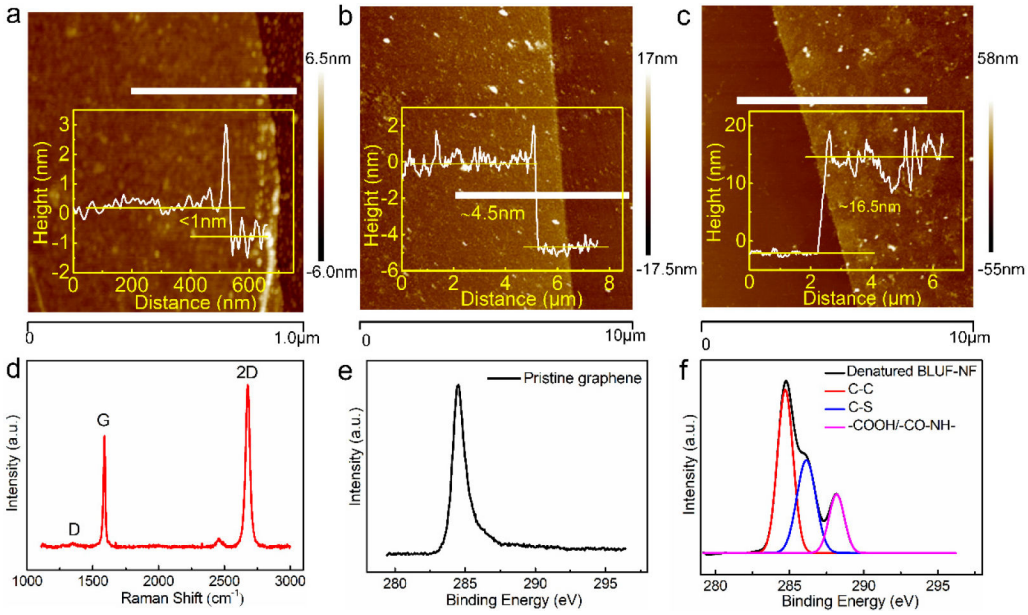

Figure 2.

The characterization results in the modification processes. (a) The AFM image of pristine graphene. Inset shows the thickness of pristine graphene is approximately 1 nm when measured along the horizontal white line in AFM image. (b) The AFM image of the thermal denatured BLUF-NF films on graphene surface. Inset shows the thickness of BLUF-NF layer is approximately 3.5 nm when measured along the horizontal white line in AFM image. (c) The AFM image of the the cross-linked BLUF-K_5 films on graphene surface. Inset shows the thickness of BLUF-K_5 layer is approximately 12 nm when measured along the horizontal white line in AFM image. (d) The Raman spectrum of pristine graphene. (e) The XPS C1s peak of pristine graphene. (f) The XPS C1s peak of the denatured BLUF-NF films on graphene surface.

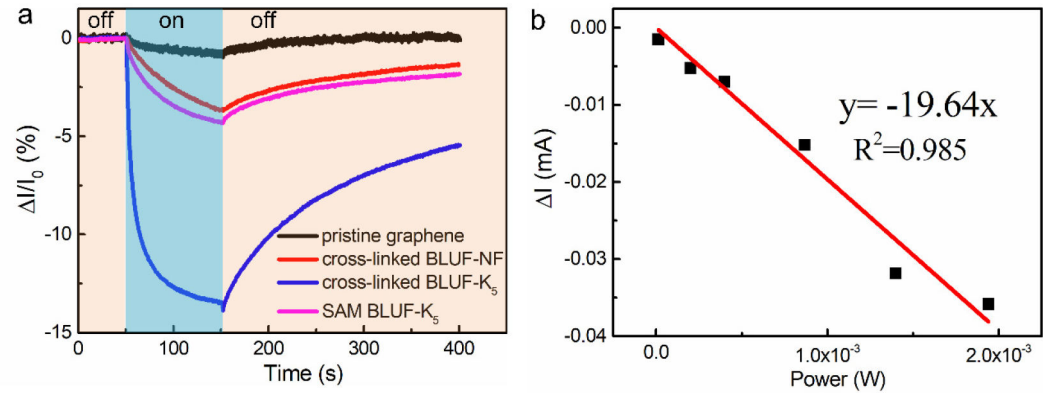

Figure 3.

(a) Photocurrent responses of detectors hybrid with different sensitive materials: pristine graphene (black), cross-linked BLUF-NF (red), cross-linked BLUF-K_5 (blue), SAM BLUF-K_5 (pink). Responses are shown to 450 nm light. (b) Power-dependent photocurrent change of the graphene photosensor functionalized with cross-linked BLUF-K_5 under 450 nm illumination.

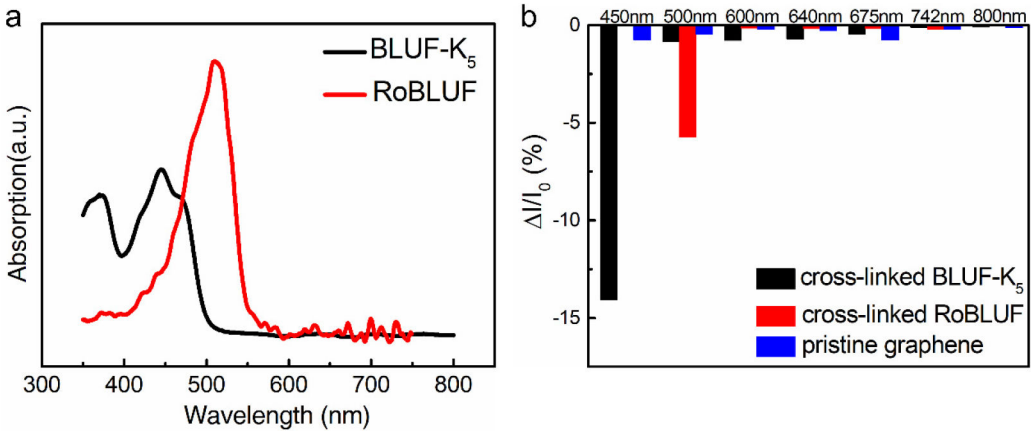

Figure 4.

(a) The optical absorption spectra of BLUF-K_5 (black) and RoBLUF (red). (b) Wavelength dependence of the photocurrent responses of detectors before and after functionalization, pristine graphene (blue), cross-linked BLUF-K_5 (black) and of cross-linked RoBLUF (red).

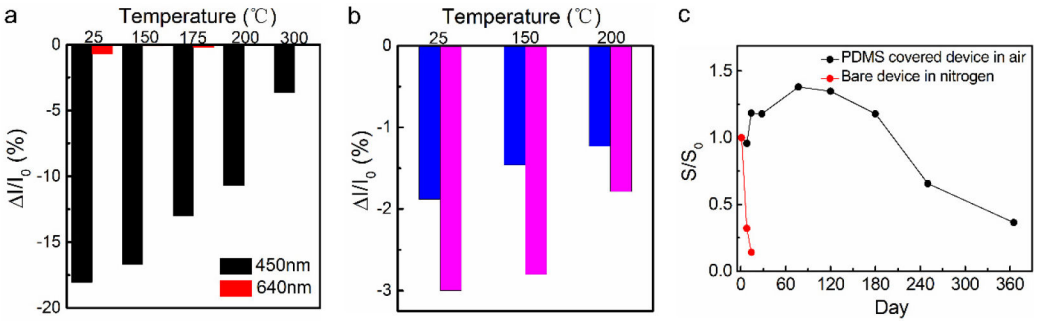

Figure 5.

(a) Comparison of the photocurrent responses of detector functionalized with cross-linked BLUF-K_5 at different temperature. (b) Comparison histogram of 450 nm photocurrent response of the graphene photosensors functionalized with free FAD (blue) or with cross-linked BLUF-NF (magenta) at different temperatures. (c) The performance to 450 nm illumination of PDMS covered device in air and bare device in nitrogen. $S = \Delta I/I_0$.

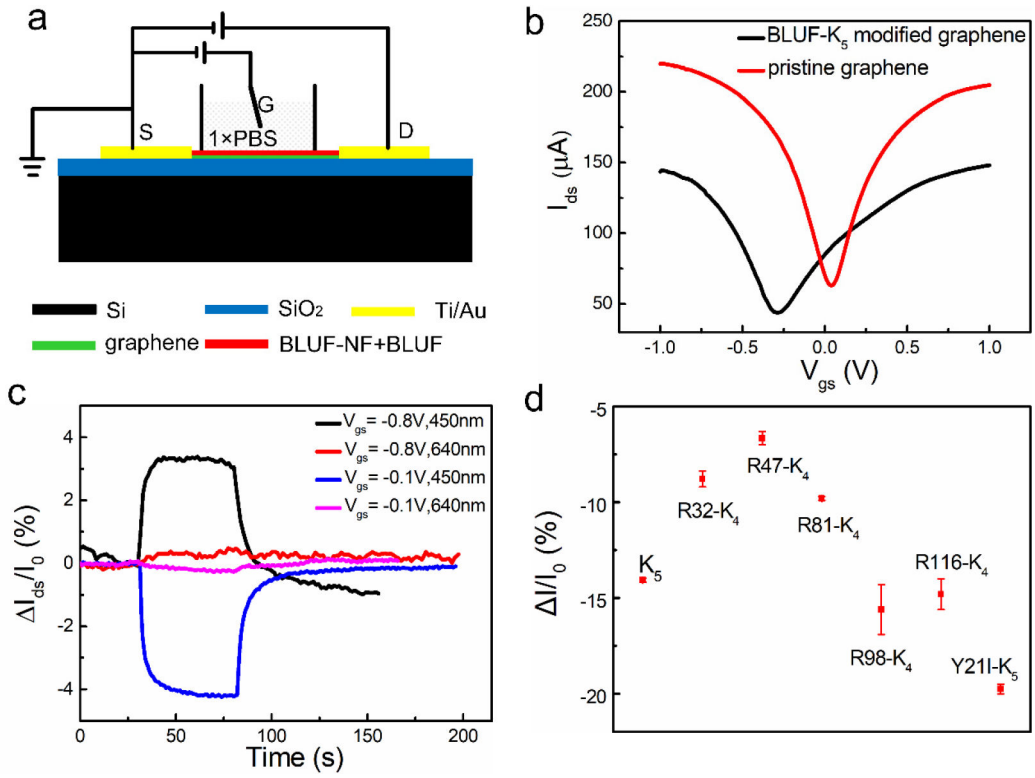

Figure 6.

(a) The schematic illustration of liquid gated graphene FET (GFET) for blue light detection. (b) Transfer curves of GFET before (red) and after modification (black). Bias voltage is 0.01 V. (c) Photocurrent responses of the modified GFET at different gate voltages. Illumination began at t=30 s and end at t=80 s. (d) Photocurrent responses of graphene detectors functionalized with various BLUF mutants.